Naval Research Laboratory

Washington, DC 20375-5320

NRL/FR/7120--04-10,088

Vertical Directionality of Low-Frequency Wind Noise and Vertical Array Optimization for the Wind Noise Limit

THOMAS J. HAYWARD
RICHARD M. HEITMEYER

Acoustic Signal Processing Branch
Acoustics Division

August 27, 2004

Approved for public release; distribution is unlimited.

REPORT DOCUMENTATION PAGE

Form Approved
OMB No. 0704-0188

Public reporting burden for this collection of information is estimate
maintaining the data needed, and completing and reviewing this collectio
suggestions for reducing this burden to Department of Defense, Washington Headquarters Services, Directorate for Information Operations and Reports (0704-0188), 1215 Jefferson Davis Highway, Suite 1204, Arlington, VA 22202-4302. Respondents should be aware that notwithstanding any other provision of law, no person shall be subject to any penalty for failing to comply with a collection of information if it does not display a currently valid OMB control number. **PLEASE DO NOT RETURN YOUR FORM TO THE ABOVE ADDRESS.**

1. REPORT DATE *(DD-MM-YYYY)*	2. REPORT TYPE	3. DATES COVERED *(From - To)*
27-08-2004	Formal Report	From 10-01 to 09-30-02

4. TITLE AND SUBTITLE

Vertical Directionality of Low-Frequency Wind Noise and Vertical Array Optimization for the Wind Noise Limit

5a. CONTRACT NUMBER

5b. GRANT NUMBER

5c. PROGRAM ELEMENT NUMBER
0602435N

6. AUTHOR(S)

Thomas J. Hayward and Richard M. Heitmeyer

5d. PROJECT NUMBER
BE-35-2-62

5e. TASK NUMBER

5f. WORK UNIT NUMBER
6701

7. PERFORMING ORGANIZATION NAME(S) AND ADDRESS(ES)

Naval Research Laboratory
4555 Overlook Avenue
Washington, DC 20375-5320

8. PERFORMING ORGANIZATION REPORT NUMBER

NRL/FR/7120--04-10,088

9. SPONSORING / MONITORING AGENCY NAME(S) AND ADDRESS(ES)

Office of Naval Research
800 North Quincy Street
Arlington, VA 22217

10. SPONSOR / MONITOR'S ACRONYM(S)
ONR

11. SPONSOR / MONITOR'S REPORT NUMBER(S)

12. DISTRIBUTION / AVAILABILITY STATEMENT

Approved for public release; distribution is unlimited.

13. SUPPLEMENTARY NOTES

14. ABSTRACT

Normal mode-based noise modeling is applied to investigate the structure and the environment dependence of vertical wind noise directionality and the optimal design of vertical arrays for detection in a wind noise background, using, as examples, two deep-water sites, one in the North Atlantic and the other in the North Pacific. The contributions to the noise directionality of the overhead (direct-path), surface-interacting, and sediment-interacting components of the noise field are examined through analysis of the vertical noise response of a reference aperture. Environmental influences investigated include the effects of (1) the wind noise source distribution in range, and (2) the acoustic propagation environment, including water-column depth and sound speed, sediment attenuation, and sea surface roughness. Spatial configurations of vertical arrays with arbitrary phone spacing are optimized by simulated annealing to maximize a measure of the mean array gain. The beam patterns of the optimized arrays adapt to the noise directionality by trading off beamwidth, sidelobe levels, and single-element signal-to-noise ratio.

15. SUBJECT TERMS

Underwater acoustics	Noise directionality	Vertical arrays	Array optimization
Ambient noise	Wind noise	Array configuration	Simulated annealing

16. SECURITY CLASSIFICATION OF:			17. LIMITATION OF ABSTRACT	18. NUMBER OF PAGES	19a. NAME OF RESPONSIBLE PERSON
a. REPORT	b. ABSTRACT	c. THIS PAGE			Thomas J. Hayward
Unclassified	Unclassified	Unclassified	UL	21	19b. TELEPHONE NUMBER *(include area code)* (202) 767-2196

Standard Form 298 (Rev. 8-98)
Prescribed by ANSI Std. Z39.18

CONTENTS

VERTICAL DIRECTIONALITY OF LOW-FREQUENCY WIND NOISE AND VERTICAL ARRAY OPTIMIZATION FOR THE WIND NOISE LIMIT

1. INTRODUCTION

The vertical directionality of the wind-generated (breaking wave) noise sensed by a vertical or volumetric array is influenced by the sea state dependent acoustic source distribution associated with breaking surface waves and by the acoustic propagation environment. In the near field of a vertical array of sufficient aperture, individual overhead breaking wave events may be spatially and temporally resolvable given sufficiently small integration times [1]. However, at ranges of more than a few kilometers, the individual breaking wave events are spatially unresolvable due to their high density in vertical angle and their extensive distribution in bearing. Thus, with the important exception of overhead noise and short integration times, the wind-generated noise sensed by a vertical array presents an angularly dispersed noise background (wind noise floor). The wind noise floor determines the detection performance limits of underwater acoustic arrays that either operate in wind-dominated noise or have sufficient horizontal aperture to reject individual shipping noise sources.

The noise gain of a vertical array is determined by the ambient noise properties, including the noise power as a function of depth and vertical angle, and by the array properties, including array depth and phone spacing, main-lobe beamwidth, and sidelobe levels. The array properties must be optimally designed, given the noise properties, to minimize the array noise gain relative to the signal gain.

This report presents the results of a modeling and optimization study that investigated the structure and the environment dependence of the vertical wind noise directionality and the optimal design and performance of vertical arrays for signal detection in a wind noise background. Two deep-water sites, one in the North Atlantic Ocean and the other in the North Pacific Ocean, were chosen. The study investigated the dependence of the vertical wind noise directionality on the wind noise source distribution in range and on the acoustic propagation environment, including water-column depth and sound speed, sediment attenuation, and surface roughness. The features of the wind noise directionality are interpreted through an examination of the contributions of overhead (direct-path), surface-reflected, and sediment- and basement-interacting propagation paths. The properties of the optimal array configurations, including the array depth and hydrophone spacing and the consequent features of the beam pattern, are interpreted in terms of the noise directionality and depth dependence.

Section 2 describes the noise modeling approach followed in the study. Section 3 describes the wind noise modeling results, including the contributions of the several propagation path classes and the dependence of the vertical wind noise directionality on the environmental parameters. Section 4 describes the array optimization approach and results and examines the impact of the vertical noise directionality on the optimal array configurations. Section 5 provides a summary of the results and concluding remarks.

2. NOISE MODELING APPROACH

The acoustic environments for the study were obtained from archival bathymetric, sound speed, and geoacoustic databases. An Atlantic Ocean site at 70 deg W × 30 deg N (Fig. 1) and a Pacific Ocean site at 144 deg W × 52 deg N (Fig. 2) were selected.

Manuscript approved August 28, 2003.

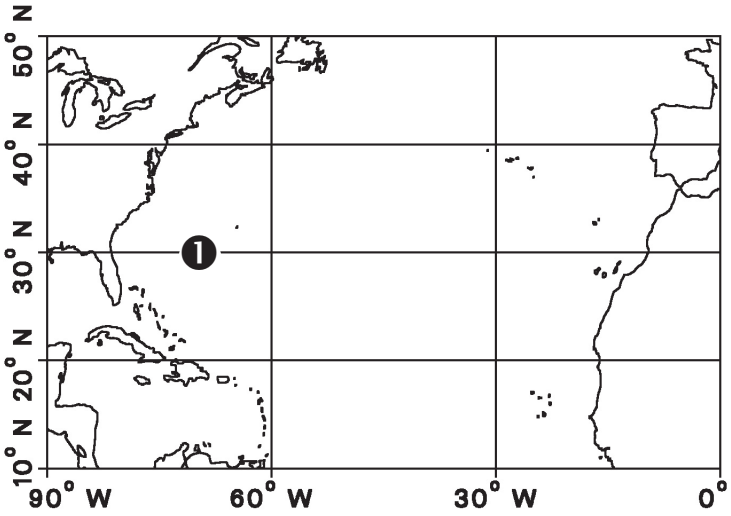

Fig. 1 — Location of site 1 (Atlantic site)

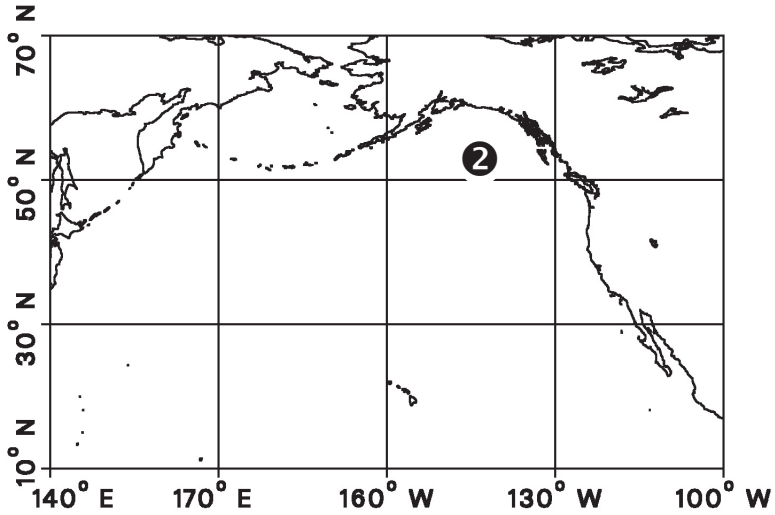

Fig. 2 — Location of site 2 (Pacific site)

Figures 3 and 4 show the water-column and sediment/basement sound speed profiles for the archival environments. In both cases, a thick sediment layer overlies a basement, which is assumed to consist of basalt and is represented by an isovelocity half-space of sound speed 4,225 m/s. For the Atlantic environment, the sediment thickness is approximately 950 m, and the sound speed minimum is located at a depth of approximately 1,340 m. For the Pacific environment, the sediment thickness is approximately 450 m, and the sound speed minimum is located at a depth of approximately 200 m. Acoustic attenuation varies with depth within the sediment, ranging from 0.005 to 0.014 dB/km-Hz in the Atlantic environment and from 0.01 to 0.17 dB/km-Hz in the Pacific environment.

Vertical array response modeling and vertical array optimization were based on range and bearing independent normal-mode computations, following the approach described in Ref. 2. The normal-mode eigenvalues and depth functions were computed using the Kraken computer code [3]. Similar normal mode-based ambient noise modeling approaches are found in Refs. 4 and 5. The long-term mean noise source distribution was represented by a near-surface (0.1-m deep) sheet of uncorrelated point sources. The mean beam response of a reference aperture to the acoustic field of the noise source distribution was computed to

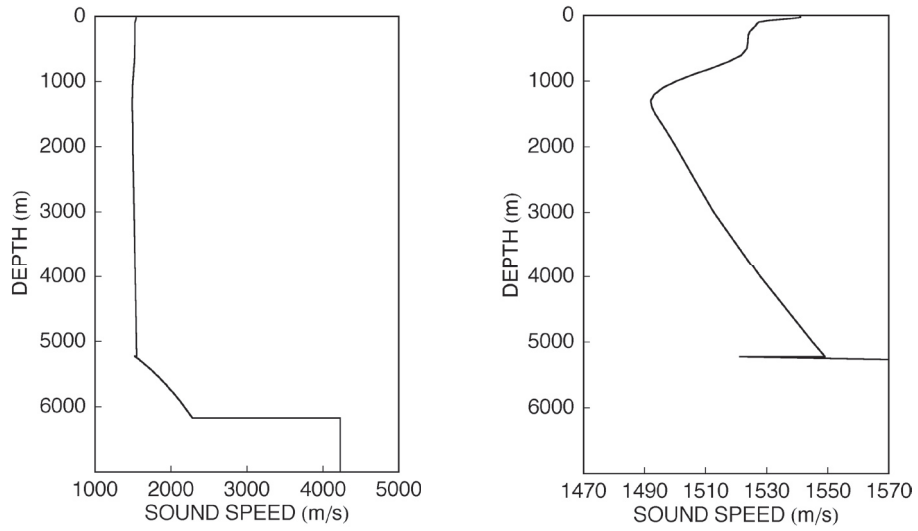

Fig. 3 — Sound speed for the archival environment at site 1 (Atlantic site):
(a) water column, sediment and basement; (b) detail of water column

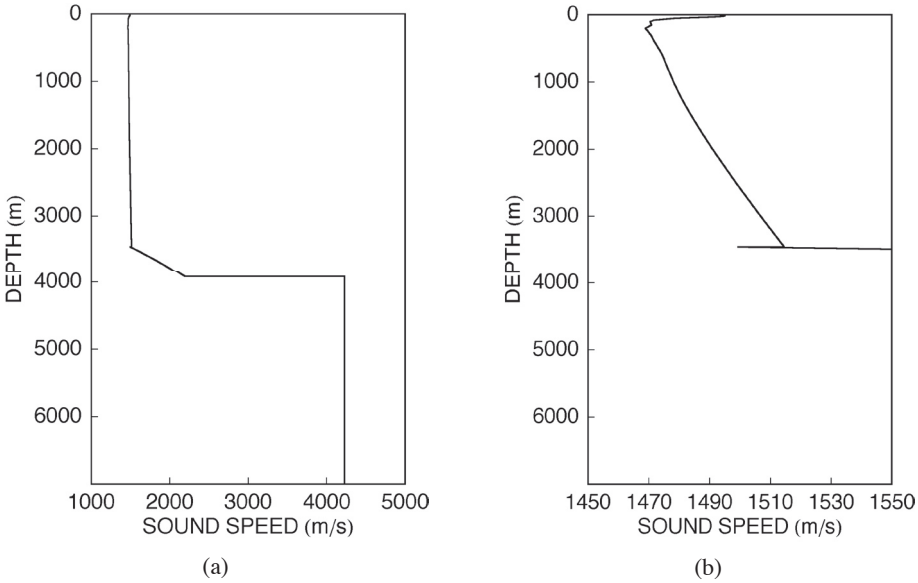

Fig. 4 — Sound speed for the archival environment at site 2 (Pacific site):
(a) water column, sediment and basement; (b) detail of water column

examine the vertical noise directionality and to provide a reference vertical-angle distribution of wind noise for interpreting the beam patterns of the optimized arrays.

3. NOISE DIRECTIONALITY

Vertical noise directionality was investigated for each site using the archival environments. Model computations for the Atlantic and Pacific sites were compared to note the effects on the noise directionality of water-column and sediment refraction, interface reflection, and sediment attenuation. The dependence of the vertical noise directionality on sea surface roughness was then examined for the Pacific site. A frequency

of 200 Hz was chosen as representative of the low-frequency regime; however, to indicate the frequency dependence of the noise directionality, Section 3.5 presents noise modeling results for 50, 100, 200, and 400 Hz.

Computations were performed for two model noise source distributions, representing two generic wind conditions. Figure 5(a) illustrates a condition of relatively high local wind speed, with areas of comparable wind speed distributed at a distance from the array; this condition is represented in the model computations by a uniform distribution of sources over a disc (Fig. 5(b)). Figure 5(c) illustrates a condition of relatively low local wind speed with areas of higher wind speed distributed at a distance from the array; this condition is represented by a uniform distribution of sources over an annular region (Fig. 5(d)). These conditions will be referred to as "local+distant" and "distant" wind conditions, respectively.

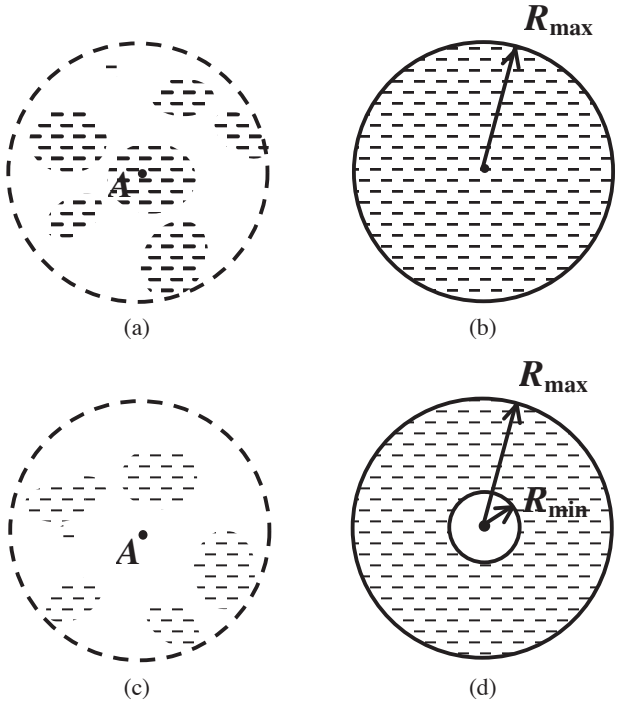

Fig. 5 — Schematic illustration of wind noise source distributions (overhead view) and their model representations: (a) local+distant wind; (b) model local+distant noise source distribution; (c) distant wind; (d) distant noise source distribution

For the present study, we fixed R_{max} = 5,000 km, and selected R_{min} = 0 and 20 km to represent the local+distant and distant wind conditions, respectively. Preliminary computations indicated that the general features of the noise directionality are not strongly dependent on the choices of the source range limits, and that the chosen range limits provide a general indication of the dependence of the vertical directionality on the noise source distribution in range. To measure the vertical noise directionality, model computations were performed to compute the mean beam responses of a reference vertical array having a length of 80 m (a little more than 10 wavelengths), consisting of 33 elements spaced at intervals of 2.5 m. Figure 6 shows the modeled beam responses of the reference array to local+distant wind noise when the array is centered at depths of 50 m (Fig. 6(a)) and 500 m (Fig. 6(b)) at the Atlantic site. Note that the angular width of the low-angle "noise notch" varies significantly with array depth, while the beam response at higher angles is only weakly depth dependent. This can be predicted from Snell's law and the sound speed structure, since the arrival angles of paths emanating from the surface at low angles vary more with receiver depth than do the arrival angles of paths emanating at higher angles.

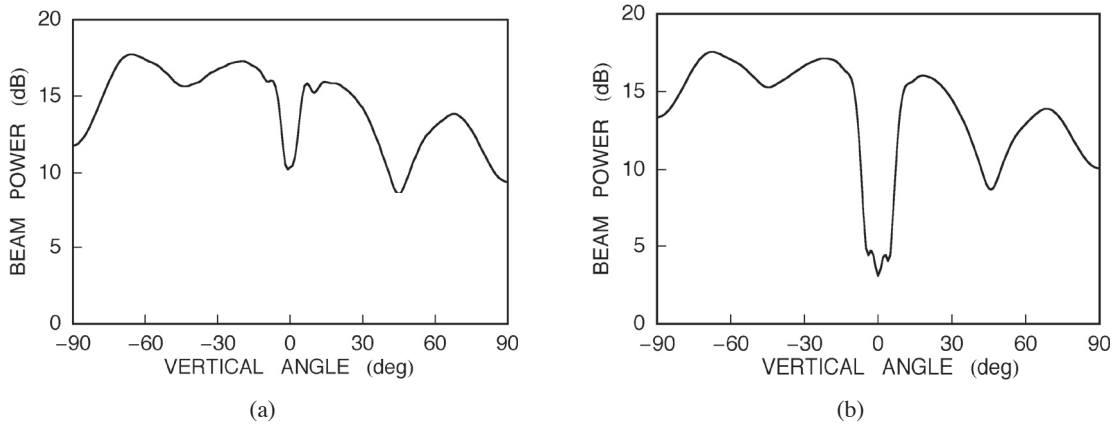

Fig. 6 — Modeled beam response of the reference array to the local+distant noise source distribution at the Atlantic site: (a) receiver depth 50 m; (b) receiver depth 500 m

The prominent features of the noise directionality, including the overhead noise component and the low-angle notch, have been described previously by several authors for both shallow- and deep-water environments [5-7]. (Reference 7 contains a fairly extensive survey and bibliography of previous work on noise directionality.) The following analyses examine the features of the vertical noise directionality for the Atlantic and Pacific deep-water environments and interpret those features through normal-mode computations and through approximate computations of ray-theoretic field intensities.

3.1 The Overhead Noise Component

A simplified model of the overhead (direct-path) component of the noise, which accounts for the vertical-angle dependence of the high-angle noise, was derived from approximations to ray-theoretic field intensity computations. These computations were performed to provide an interpretation of the subsequent normal-mode computations of the overhead noise, and to determine the integration ranges for normal mode-based computations of the direct-path and the refracted, surface-reflected (RSR) components of the noise.

The computation is illustrated in Fig. 7(a). (Other ray-based noise models, which provide computations of noise coherence in addition to noise directionality, have been documented previously [8,9].) A uniform sheet of uncorrelated dipole sources is assumed to lie at the surface. The dipole source approximates the contribution that a monopole source placed near the surface would have in a computation of the complex acoustic field. Propagation paths derived from Snell's law connect the surface to the array receivers. For each vertical arrival angle θ, a recursive computation indexed by receiver depth computes the paths (if any) arriving from the ocean surface at that angle at each of the receiver depths. Spreading losses are approximated by the inverse square of the path arc length, and noise source surface area elements are computed from the ranges of intersection of the path with the noise source surface (Fig. 7(b)). Contributions from each surface element are then incoherently summed to represent the total power arriving at the array at the given vertical angle.

Curve 2 in Fig. 8 shows the modeled array response to the overhead noise, computed using the approximate ray model. (For comparison, curve 1 repeats the full noise response computed by the normal-mode model.) A vertical angle of –90 deg represents arrivals from directly overhead, while an angle of 0 deg represents horizontal arrival.

For comparison with the approximate ray model, a normal mode-based computation of the beam response to the overhead noise was obtained by integrating over noise source ranges from 0 to the maximum range of direct paths joining the receivers to the noise source surface. A large number of normal modes (941

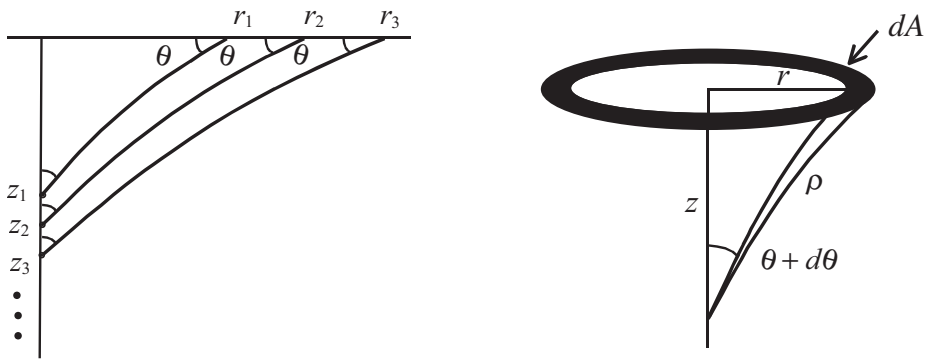

(a) (b)

Fig. 7 — (a) Illustration of paths contributing to the noise directionality at arrival angle θ for the approximate ray model of overhead noise. (b) Source area element associated with paths arriving at a high angle θ.

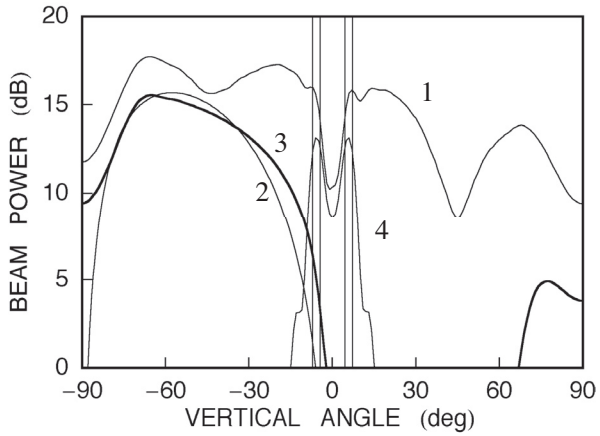

Fig. 8 — Modeled components of the beam response of the reference array to the local+distant noise source distribution at the Atlantic site: Curve 1 — full directional response; Curve 2 — approximate ray model of overhead component; Curve 3 — normal-mode model of overhead component; Curve 4 — normal-mode component of RSR component. Vertical lines mark the boundaries of the arrival angle intervals corresponding to RSR paths.

for the Atlantic site) were computed to include the high-angle energy needed for modeling the overhead noise component. (Comparisons with fast-field program (FFP) computations of the acoustic field were made to confirm the accuracy of the normal-mode representation at short ranges.) Sediment-interacting energy was eliminated by prolonging the water-column sound speed profile into an isovelocity half-space with sound speed equal to the sound speed in the water column at the water/sediment interface. Curve 3 in Fig. 8 shows the resulting beam response. Comparing the approximate ray model result with the more detailed normal mode-based computation shows that the approximate ray model provides a good approximation to the angular dependence of the normal mode-modeled overhead noise. Minor differences may result from several effects not included in the approximate ray model, including coherent multipath interference and beamforming effects.

Note that the approximate ray model predicts that the power density per unit of vertical angle of the overhead noise will vanish at an angle of –90 deg (i.e., directly overhead). This occurs because the derivative, with

respect to vertical angle, of the acoustic source area approaches 0 as the vertical angle approaches –90 deg. More explicitly, Fig. 7(b) indicates that the following approximations may be used for small angles θ:

$$r = z \tan\theta; \quad \rho = z \sec\theta; \quad dA = 2\pi r dr. \tag{1}$$

The acoustic field power dI received at depth z and at range r from an acoustic source having unit source density over the elemental area dA is then given by

$$\begin{aligned} dI &= dA / \rho^2 = 2\pi r\, dr / \rho^2 = 2\pi \cdot z \tan\theta \cdot d(z\tan\theta) / z^2 \sec^2\theta \\ &= 2\pi \tan\theta\, d\theta, \end{aligned} \tag{2}$$

so that

$$dI / d\theta = 2\pi \tan\theta \to 0 \text{ as } \theta \to 0. \tag{3}$$

This limiting behavior near the vertical also accounts for the decay at high angles of the normal mode-modeled overhead noise (curve 3 in Fig. 8). However, in the normal-mode model, the effect of the finite aperture produces a finite beam response at the vertical.

3.2 The Low-Angle Noise Notch and Dual Noise Peaks

For a receiver placed at a depth at which the sound velocity is less than that at the surface, refraction in the water column produces a "noise notch" (previously noted in Ref. 5 and elsewhere) resulting from the virtual absence of surface-generated noise arriving at angles below the arrival angles, $\pm\theta_{sur}$, of the upward and downward arriving grazing paths to the surface. The vertical-angle intervals bounded by $\pm\theta_{sur}$ and the arrival angles, $\pm\theta_{sed}$, of the grazing paths to the water/sediment interface, represent the intervals of propagation paths that interact with the surface but not with the sediment (i.e., RSR paths). Depending on the intensity of the noise arriving in these angular intervals, there may be dual peaks in the beam noise response in these intervals.

The angles $\pm\theta_{sur}$ and $\pm\theta_{sed}$ for the Atlantic environment are marked by vertical lines in Fig. 8. For the Atlantic environment, θ_{sur} = 3.9 deg and θ_{sed} = 7.1 deg. Small peaks in the noise beam response (curve 1 in Fig. 8) appear to correspond to this interval of angles. To confirm this correspondence, the response to the noise propagated only along RSR paths was computed by prolonging the water-column sound speed profile into an isovelocity half-space to extinguish all acoustic energy that interacts with the sediment. The overhead component of the noise was excluded by taking the lower limit of range-integration in the noise model to be the maximum range of the direct paths to the surface. The resulting noise beam response, curve 4 in Fig. 8, shows strong peaks in the two vertical-angle intervals. In the full noise response, these peaks are partially concealed by the noise propagated along higher-angle paths.

Figure 9 shows the beam response to local+distant wind noise for the Pacific site for receiver depths of 50 m (Fig. 9(a)) and 500 m (Fig. 9(b)). Note that the dual peaks bounding the noise notch are much more prominent for the Pacific environment. This is due in part to the larger span of launch angles associated with the RSR paths for the Pacific environment (0 to 9.3 deg for the Pacific environment vs 0 to 5.9 deg for the Atlantic environment). This results in more ensonification of the RSR paths by the effective dipole sources associated with the near-surface source sheet.

Figure 10 shows the modeled components of the beam response to the local+distant wind noise source distribution for the Pacific site. Curve 1 shows the approximate ray model of the overhead component; curve 2 shows the normal-mode model of the overhead component; and curve 3 shows the normal-mode model of

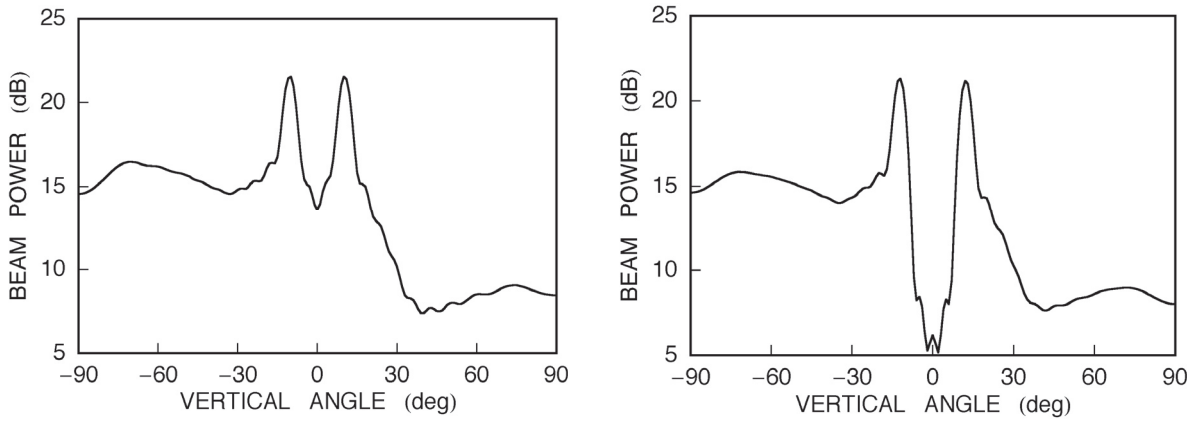

Fig. 9 — Modeled beam response of the reference array to the local+distant noise source distribution at the Pacific site for (a) array center depth 50 m; (b) array center depth 500 m

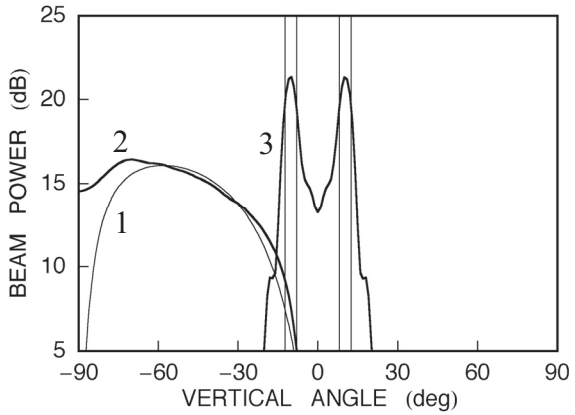

Fig. 10 — Modeled components of the beam response of the reference array (center depth 50 m) to the local+distant noise source distribution at the Pacific site: Curve 1—approximate ray model of overhead component; Curve 2—normal-mode model of overhead component; Curve 3—normal mode model of RSR component. Vertical lines mark the boundaries of the arrival angle intervals corresponding to RSR paths.

the RSR component. Vertical lines mark the boundaries of the arrival angle intervals corresponding to RSR paths. Again, the approximate ray and normal-mode models of the overhead component agree well, and the dual peaks in the RSR component of the noise align with the arrival angle intervals bounded by the grazing paths to the surface and sediment.

3.3 Sediment- and Basement-Interacting Noise; Source Range Dependence of the Noise

For the Atlantic environment, there is a significant amount of noise energy propagating along sediment-interacting (water/sediment and sediment/basement interface reflected and sediment refracted) paths. In Fig. 8, this noise is represented by the excess of the total noise beam response (curve 1) over the sum of the overhead and RSR components (curves 3 and 4). Figure 11 shows the total beam response (curve 1), together with the beam responses to RSR (curve 2), surface- and sediment-interacting (curve 3), and surface- and sediment-interacting and basement-reflected energy (curve 4). The overhead noise accounts for the

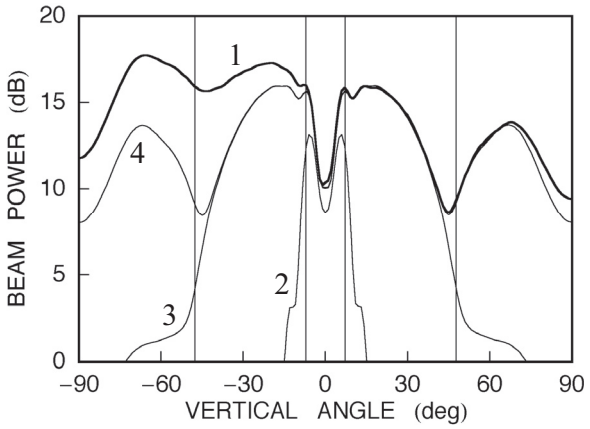

Fig. 11 — Modeled components of the response of the reference array to local+distant wind noise for the Atlantic site. Curve 1—total beam response; Curve 2—response to RSR energy; Curve 3—response to surface- and sediment-interacting energy; Curve 4—response to surface- and sediment-interacting and basement-reflected energy.

difference between curve 4 and curve 1. The vertical lines mark the arrival angles of the grazing paths to the water/sediment interface (±7.1 deg) and to the sediment/basement interface (±47.6 deg). Within this angular interval, there is a substantial component of the noise energy that is propagated along sediment-borne paths; this noise component falls off rapidly above ±30 deg (curve 3). In addition, there is a substantial contribution from paths reflected from the sediment-basement interface (vertical angles 47.6 to 90 deg (curve 4)).

For the Pacific site, there is less noise energy propagated along sediment-interacting paths, especially in relation to the waterborne noise. Figure 12 shows the total beam response (curve 1), together with the beam responses to RSR (curve 2), surface- and sediment-interacting (curve 3), and surface- and sediment-interacting and basement-reflected noise (curve 4). The vertical lines mark the grazing angles to the water/sediment interface (±12.5 deg) and to the sediment/basement interface (±47.6 deg). The sediment-borne noise falls off rapidly with vertical angle, and there is little reflection from the sediment/basement interface (compare curves 3 and 4).

Analysis of the depth functions and the range decay of the mode amplitudes in the normal-mode representation of the acoustic field can facilitate understanding of the range-dependent influences of water-column and sediment refraction, sediment and basement reflection, and sediment attenuation on the noise directionality [10]. The normal-mode representation expresses the acoustic field, sensed at receiver depth z, of a point source of unit source level at range r from the receiver and depth z_s as a sum of m modal fields, viz.,

$$\psi(z,r) = \sum_{m=1}^{M} \psi_{(m)}(z,r), \tag{4}$$

where

$$\psi_{(m)}(z,r) = \frac{\sqrt{2\pi}}{\rho(z_s)} k_m^{-1/2} \psi_m(z) \psi_m(z_s) r^{-1/2} e^{-ik_m r}. \tag{5}$$

Here k_m and ψ_m are the eigenvalue and depth function for the mth mode. For an annular source element of unit source density, lying at depth z_s and spanning ranges r to $r + dr$, the noise power of the mth modal field at range 0 and depth z is given by

$$\left|\psi_{(m)}(z,r)\right|^2 \cdot 2\pi r\, dr = \frac{4\pi^2}{\rho(z_s)^2} \left|k_m\right|^{-1} \left|\psi_m(z_s)\right|^2 e^{-2\alpha_m r} \left|\psi_m(z)\right|^2 dr, \tag{6}$$

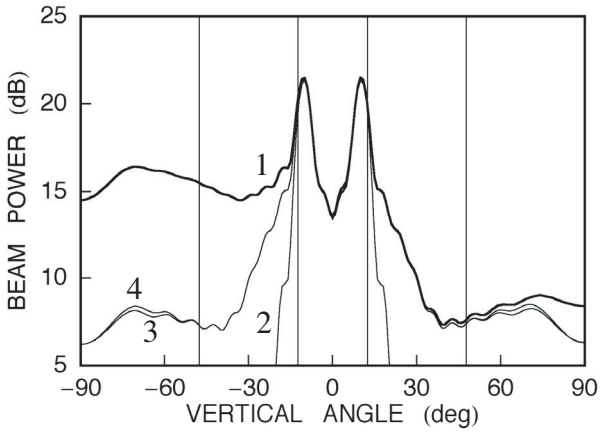

Fig. 12 — Modeled components of the response of the reference array to local+distant wind noise for the Pacific site. Curve 1—total beam response; Curve 2—response to RSR energy; Curve 3—response to surface- and sediment-interacting energy; Curve 4—response to surface- and sediment-interacting and basement-reflected energy.

where $\alpha_m = -\mathrm{Im}(k_m)$ is the attenuation coefficient of the mth mode. Letting

$$A_m^2(r) = \frac{4\pi^2}{\rho(z_s)^2} |k_m|^{-1} |\psi_m(z_s)|^2 \, e^{-2\alpha_m r}, \tag{7}$$

Eq. (6) becomes

$$|\psi_{(m)}(z,r)|^2 \cdot 2\pi r \, dr = A_m^2(r) |\psi_m(z)|^2 \, dr. \tag{8}$$

Thus, the contribution to the noise power, via the mth mode, of the annular source element spanning ranges r to $r + dr$ is expressed as the product of a range-dependent amplitude squared and the magnitude squared of the mth modal depth function.

Figure 13 shows the normalized modal depth functions and the range decay of the corresponding amplitudes $A_m(r)$ for the Atlantic site, plotted as a function of mode number. More explicitly, a vertical section of Fig. 13(a) represents, for a fixed mode number m, the function 10 log $|\psi_m(z)|^2$. Vertical lines in Fig. 13(a) partition the modes into RSR, sediment-interacting, and sediment- and basement-interacting mode sets. A vertical section of Fig. 13(b) represents, for a fixed mode number m, the function 20 log $A_m(r)$. Thus, Fig. 13(b) provides a visual overview of the contributions of the different modes to the ambient noise as a function of source range. Figure 13(b) confirms the relatively weak contribution of noise propagated along RSR paths for the Atlantic site.

Figure 14 shows the same functions for the Pacific site. Figure 14(b) confirms the stronger contribution of noise propagated along RSR paths for the Pacific site; in fact, the RSR paths contribute significantly to the low-angle noise peaks to ranges of 5,000 km or more. The sediment-borne noise decays somewhat more rapidly with range than at the Atlantic site, due to the higher attenuation in the sediment in the Pacific environment. However, it is the RSR energy that accounts for most of the difference in the vertical noise directionality between the two sites. Note, also, that the modal depth functions attenuate more strongly with depth for the Pacific environment than for the Atlantic environment, again due to the higher sediment attenuation. This appears to account for the smaller contribution of basement-reflected energy to the noise field at the Pacific site.

To illustrate the different constituency of distant noise for the two environments, the vertical directionality of distant noise was computed. Figures 15 and 16 show beam responses to the distant (20 to 5,000 km)

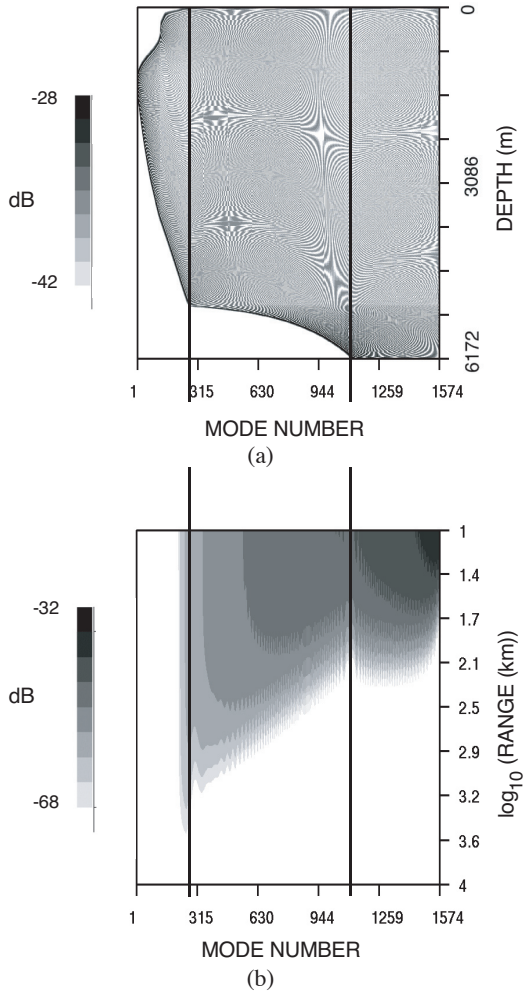

Fig. 13 — (a) Normal-mode depth functions plotted as a function of mode number and depth for the Atlantic environment. (b) Modal field power multiplied by elemental source surface area, plotted as a function of mode number and range. Vertical lines partition the modes into waterborne, sediment-interacting, and sediment- and basement-interacting mode sets.

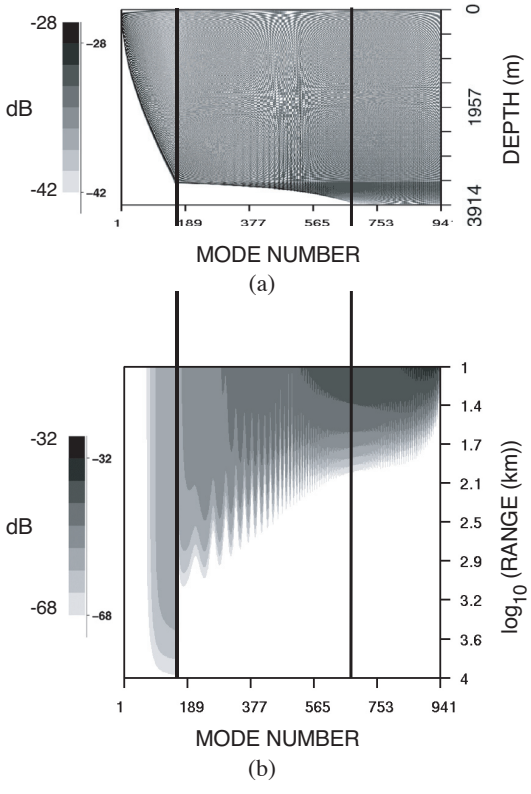

Fig. 14 — (a) Normal-mode depth functions plotted as a function of mode number and depth for the Pacific environment. (b) Modal field power multiplied by elemental source surface area, plotted as a function of mode number and range. Vertical lines partition the modes into waterborne, sediment-interacting, and sediment- and basement-interacting mode sets.

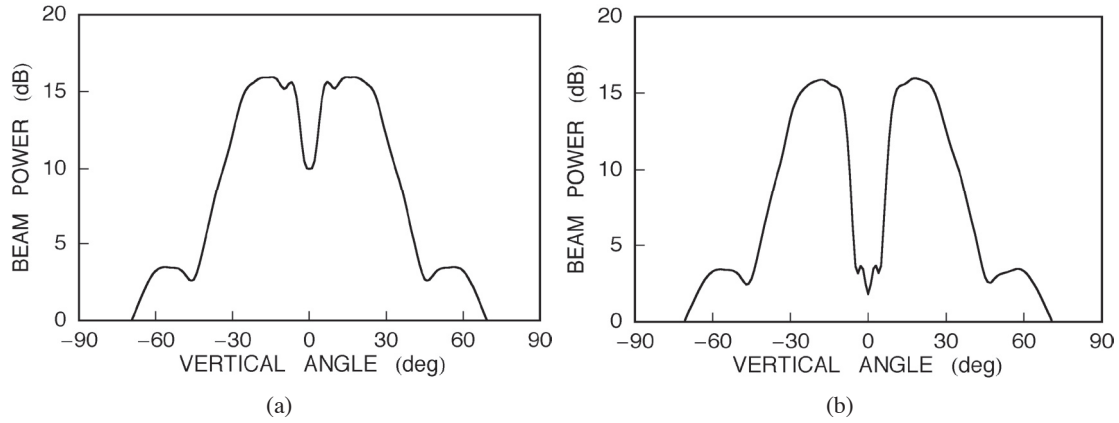

Fig. 15 — Modeled response of the reference array to distant wind noise for the Atlantic site: (a) array center depth 50 m; (b) array center depth 500 m

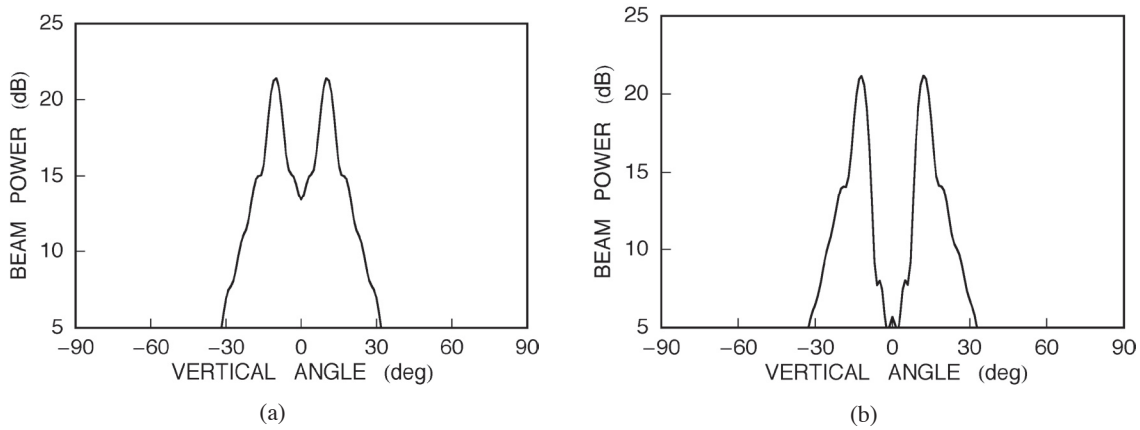

Fig. 16 — Modeled response of the reference array to distant wind noise for the Pacific site: (a) array center depth 50 m; (b) array center depth 500 m

noise source distribution for the Atlantic and Pacific environments, respectively. Comparison with Figs. 10 and 11 shows that, for the Pacific site, the distant noise is carried predominantly by RSR paths, whereas, for the Atlantic site, the sediment-borne components dominate the distant noise.

3.4 Effect of Surface Roughness

Figure 17 shows the effect of surface roughness on the noise response of the reference array. The lighter curve shows the beam response in the absence of surface roughness for the reference array when centered at a depth of 50 m at the Pacific site. The heavier curve shows the beam response for an rms surface roughness of 2 m, obtained using a perturbation theory-based computation of the effect of the surface roughness on the normal-mode acoustic field [3,11]. Note that the low-angle peaks in the noise response, which are predominantly associated with distant noise sources, are substantially attenuated by extensive interaction with the rough surface.

3.5 Frequency Dependence of the Vertical Noise Directionality

To examine the frequency dependence of the vertical noise directionality, the responses of reference vertical arrays to the local+distant noise source distribution were simulated for frequencies of 50, 100, 200, and 400 Hz. For each frequency, the reference aperture used previously for the 200-Hz noise computations

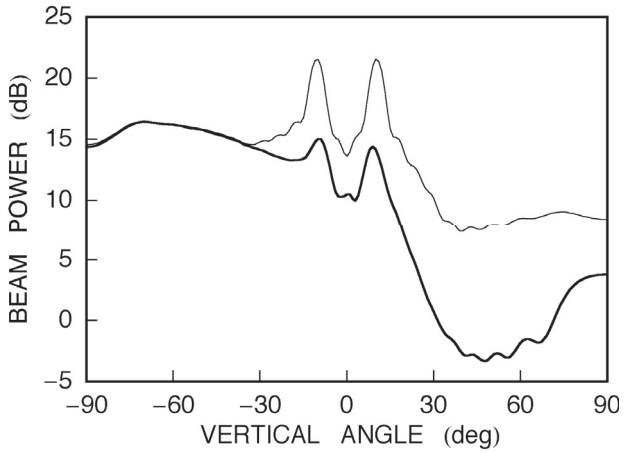

Fig. 17 — Modeled response of the reference array (center depth 50 m) to local+distant wind noise for the Pacific site. Light curve: 0-m rms surface roughness; heavy curve: 2-m rms surface roughness.

was scaled in proportion to wavelength, while the array center was maintained at a depth of 500 m. Figure 18 shows the simulated array noise responses at these frequencies for the Atlantic and Pacific sites. For the Pacific site, a 1-m rms surface roughness was assumed in order to include the effect of the surface roughness on the prominent low-angle peaks. For both sites, the qualitative aspects of the more prominent features of the noise directionality are preserved across the frequency band, but the boundary- and sediment-interacting noise components are increasingly attenuated with frequency.

4. VERTICAL ARRAY OPTIMIZATION

The preceding computations illustrate the influence on the vertical noise directionality of the noise source distribution, water-column sound speeds, acoustic attenuation in the sediment, and sea surface roughness. This section examines the impact of the noise directionality and depth dependence on optimal vertical array design by optimizing vertical array configurations for the propagation environments and signal and noise source distributions studied above. The purpose of this brief study is to investigate the correspondence between the essential features of the optimized arrays, including array depth and hydrophone spacing, beamwidth and sidelobe levels, and the features of the noise directionality and depth dependence.

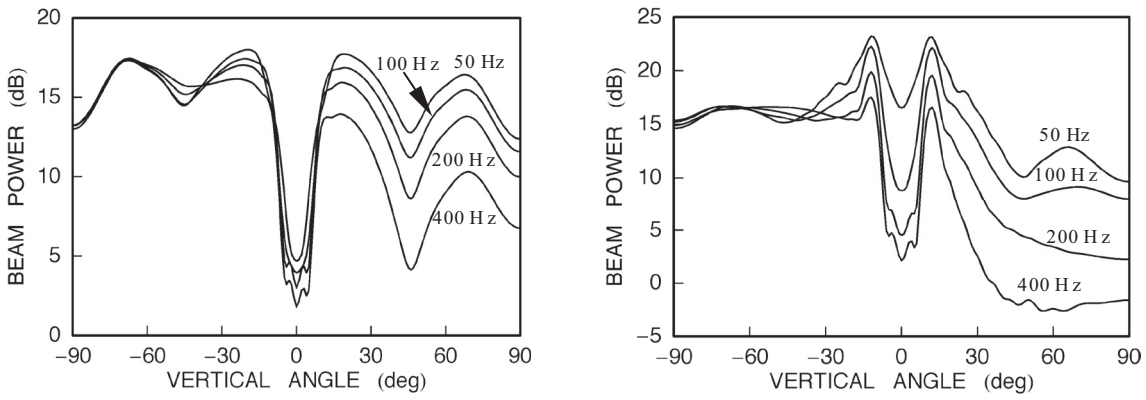

Fig. 18 — Modeled response of the wavelength-scaled reference arrays (center depth 500 m) at 50, 100, 200, and 400 Hz: (a) Atlantic site; (b) Pacific site. For the Pacific site, a 1-m rms surface roughness was assumed.

The array optimization followed the normal mode-based formulation of Ref. 2. The signal source location was represented by a probability density function that is uniform in a washer-shaped volume (Fig. 19). The array was assumed to be conventionally beamformed and steered to the horizontal. The mean array signal and noise beam responses were computed by integrating the element-pair cross-spectra over the signal and noise source distributions. Equation (33) of Ref. 2 provides a closed-form expression for these mean beam responses in terms of the normal-mode depth functions evaluated at the hydrophone depths. The array performance measure was the quotient of the mean array signal power divided by the mean array noise power, taken over the signal and noise source distributions. The array configurations were optimized by simulated annealing [2,12].

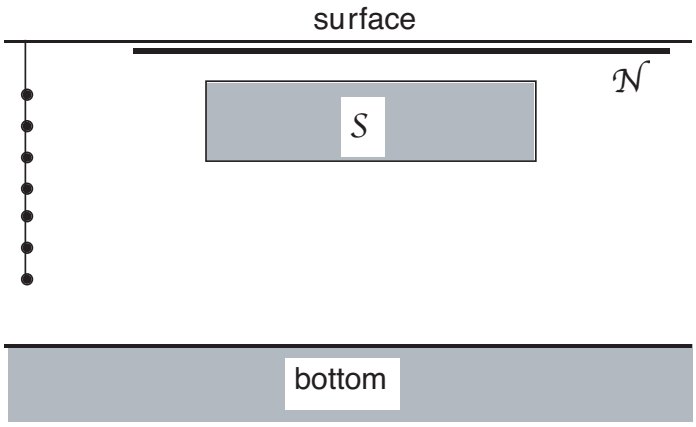

Fig. 19 — Schematic range-depth cross-section illustrating the locations, relative to the vertical array, of the noise source distribution on a surface of revolution N near the ocean surface and the signal source distribution in the volume of revolution S.

The first two optimizations examine the dependence of the optimized array and its beam pattern on the signal source depth. In the first optimization, the signal source locations were assumed to be uniformly distributed over depths of 490 to 510 m and ranges of 0 to 1000 km. (To facilitate both the exposition and the relevant graphical comparisons, the following text refers to some of the figures out of alphanumeric order.) Figure 20(a) shows the depth dependence of the point-receiver signal-to-noise ratio (SNR) and the array element locations for the optimized 7-element array for the Atlantic local+distant wind noise environment. As was observed in Ref. 2, the optimized array is centered approximately at the location of the peak SNR. The element spacing increases toward the ends of the array; the average spacing is substantially less than one-half wavelength (5.6 m vs 7.5 m for half-wavelength spacing). Figure 21(a) shows the vertical beam pattern of the optimized array and the beam noise response of an 80-m-long reference array centered at 500-m depth. The main lobe of the beam pattern fits the noise notch, and the short aperture and "tapered" element spacing provide low sidelobes in the high-noise directions.

Figure 20(b) shows the SNR depth dependence and the optimized 7-element array for signal source depths of 40 to 60 m in the Atlantic environment. Again, the array is centered near the SNR peak. The average element spacing approaches one-half wavelength (6.8 m vs 7.5 m for half-wavelength spacing). Figure 21(b) shows the vertical beam pattern of the optimized array and the noise response. The longer aperture provides a narrower main beam that fits the narrower noise notch, at the expense of high sidelobes at the vertical, where the noise power is low.

Thus, the two optimizations provide a fit of the main beam width to the depth-dependent noise notch width, while maintaining low sidelobe levels in the directions of the high-noise peaks.

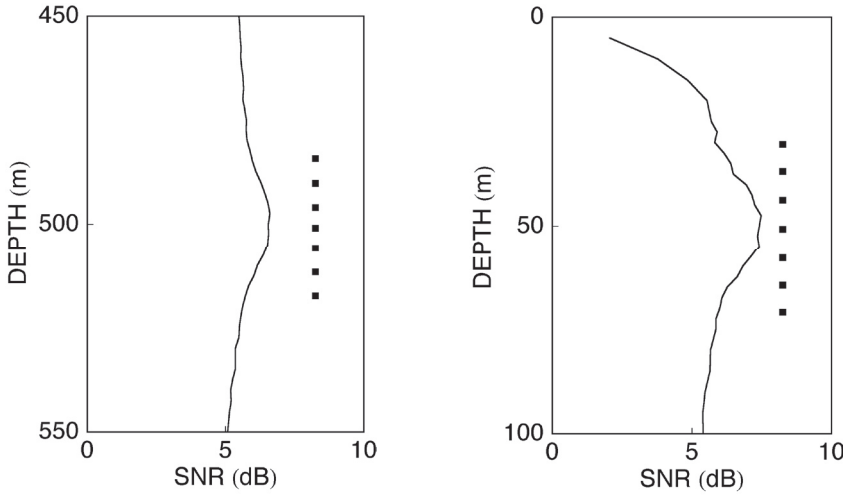

Fig. 20 — SNR depth dependence and optimized 7-element arrays for the Atlantic local+distant wind environment: (a) signal source depths 490 to 510 m (b) signal source depths 40 to 60 m

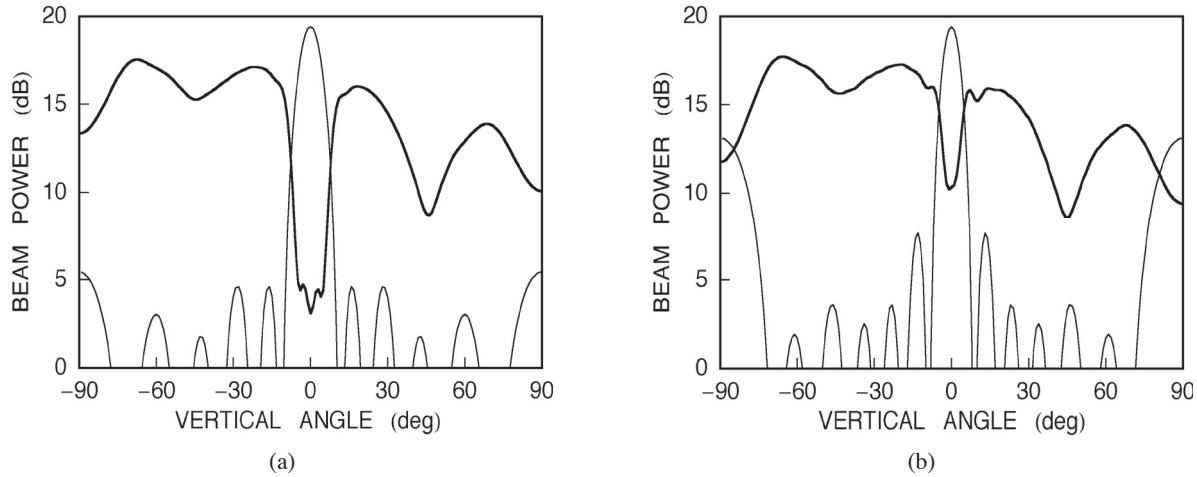

Fig. 21 — Reference array noise response (heavy curves) and vertical beam patterns (light curves) of the optimized arrays for the Atlantic local+distant wind environment: (a) signal source depths 490 to 510 m; (b) signal source depths 40 to 60 m

The next two optimizations examine the influence of the noise source range distribution on the optimal array phone spacing and beam pattern. Figure 22(a) shows the SNR depth dependence and the optimized 7-element array for the Pacific distant noise source distribution (20- to 5,000-km noise source ranges) for signal source depths of 40 to 60 m. The array is again centered near the SNR maximum. The element spacing becomes much wider toward the ends of the array and exhibits irregularity that may be influenced in part by the SNR depth variations.

Figure 23(a) shows the vertical beam pattern of the optimized array and the noise response for the distant noise source distribution. The element spacing of the optimized array produces a beam pattern that strongly suppresses the low-angle (sediment-borne) noise at the boundaries of the noise notch, at the expense of high sidelobes at the higher angles, where the noise power is negligible.

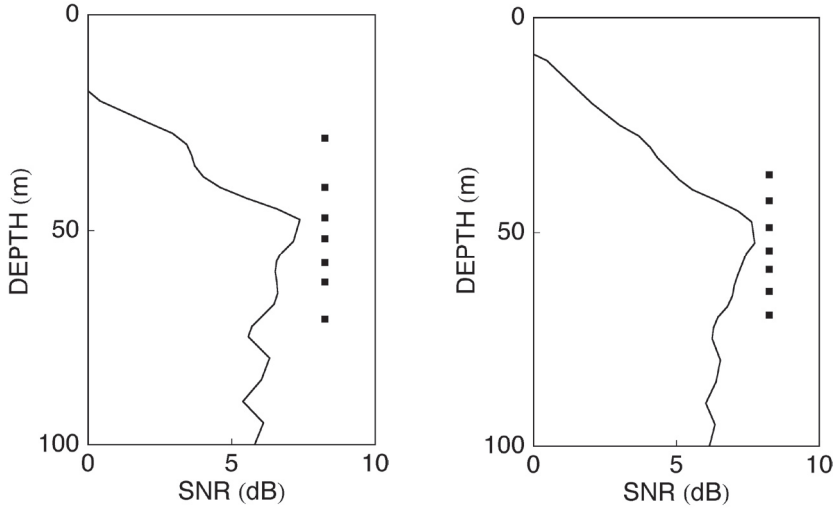

Fig. 22 — SNR depth dependence and optimized 7-element arrays for signal source depths of 40 to 60 m in the Pacific environment: (a) distant wind; (b) local+distant wind

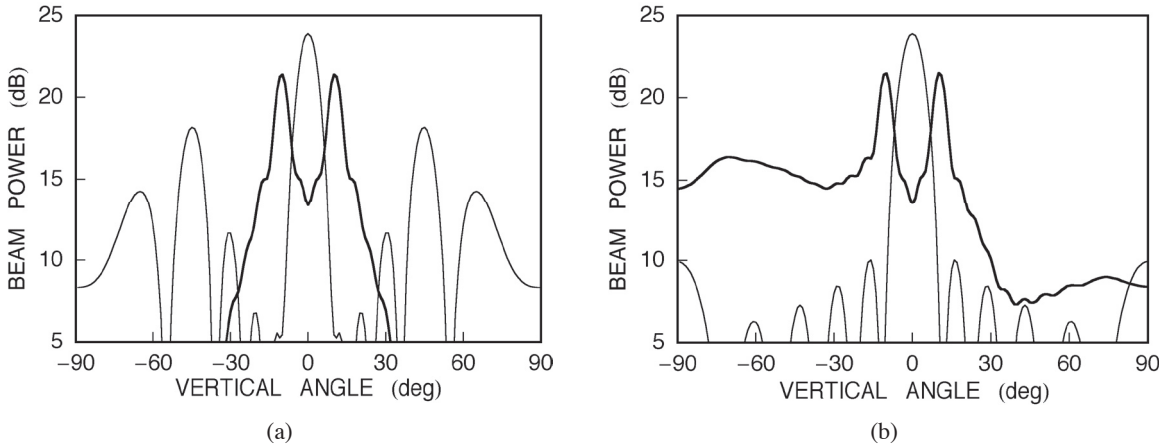

Fig. 23 — Reference array noise response (heavy curves) and vertical beam patterns (light curves) of the optimized arrays for signal source depths of 40 to 60 m in the Pacific environment: (a) distant wind; (b) local+distant wind

Figure 22(b) shows the SNR depth dependence and the optimized array for signal source depths of 40 to 60 m in the Pacific local+distant (0 to 5,000 km) noise source distribution. Figure 23(b) shows the vertical beam pattern of the optimized array and the noise response. The shorter array aperture provides sidelobe levels that strongly suppress the noise in the direction of the overhead noise peak and provide less suppression of the less-intense sediment-borne arrivals. Note that the main lobe for the Pacific local+distant noise environment is wider than for the Atlantic local+distant noise environment, corresponding to the wider noise notch (compare Fig. 23(b) with Fig. 21(b)), and the array aperture is correspondingly shorter (compare Fig. 22(b) with Fig. 20(b)).

These examples indicate that the beam patterns of the optimized arrays adapt to the noise directionality by trading off beamwidth, sidelobe levels, and SNR depth dependence. The optimal phone spacing may or may not vary significantly from uniform spacing, depending on details of the vertical noise directionality and depth dependence.

5. CONCLUDING REMARKS

A modeling and optimization study was performed to investigate the structure and the environment dependence of the vertical wind noise directionality and the optimal design of vertical arrays, using as examples two deep-water sites, one in the North Atlantic and the other in the North Pacific.

Normal mode-based modeling of the vertical noise response of a reference aperture was applied to examine the contributions of direct, surface-interacting, and sediment-interacting propagation paths to the vertical noise directionality. The results show that acoustic energy propagated along each type of path contributes distinct features to the vertical noise directionality. Computations of the overhead (direct-path) noise component, based on approximations to ray-theoretic field intensities, provide a good approximation to, and an interpretation of, the normal-mode computation of the angular dependence of the overhead noise power. Waterborne, surface-interacting (RSR) paths contributed sharp peaks in the vertical noise directionality at the boundaries of the noise notch. The levels of these low-angle peaks were significantly influenced by water-column refraction and by sea surface roughness. The contribution of sediment-borne and basement-reflected acoustic energy to distant noise was the dominant contribution for the Atlantic environment, which has low acoustic attenuation values in the sediment layer, but was significantly smaller for the Pacific environment, which has higher sediment attenuation values.

Spatial configurations of non-uniformly spaced vertical arrays were optimized by simulated annealing to maximize a measure of the mean array gain computed by a normal mode-based signal and noise model. The beam patterns of the optimized arrays adapted to the noise directionality by trading off beamwidth, sidelobe levels, and SNR depth dependence. Examples showed that the spacing of the optimized vertical arrays may or may not vary substantially from uniform spacing, depending on the vertical noise directionality and, secondarily, the depth dependence of the noise power.

The results of this study indicate that the features of the vertical noise directionality in deep water may be sensitive to environmental parameters, the values of which may not be known with a high degree of certainty over the relevant ocean region. This emphasizes the need for either improved measurements of the relevant environmental parameters, or alternatively, analysis of the implications of environmental uncertainty for noise prediction and for array design and performance prediction.

ACKNOWLEDGMENTS

This work was performed as part of a joint research effort by the Johns Hopkins University Applied Physics Laboratory (APL) and the Naval Research Laboratory (NRL) under funding from the Office of Naval Research (ONR) and from the ONR Base Program at NRL. The authors gratefully acknowledge helpful discussions with Dr. Iman Schurman of APL.

REFERENCES

1. S. Finette and R.M. Heitmeyer, "Angle-time-frequency Resolution of the Noise Field Generated by Wind-induced Breaking Waves," *J. Acoust. Soc. Am.* **99**, 209-222 (1996).

2. T.J. Hayward, "Optimization of Hydrophone Placement for Acoustic Arrays Using Simulated Annealing," *J. Acoust. Soc. Am.* **95**, 201-212 (1994).

3. M.B. Porter and E.L. Reiss, "A Numerical Method for Bottom Interacting Ocean Acoustic Normal Modes," *J. Acoust. Soc. Am.* **77**, 1760-1767 (1985).

4. W. Kuperman and F. Ingenito, "Spatial Correlation of Surface Generated Noise in a Stratified Ocean," *J. Acoust. Soc. Am.* **67**, 1988-1966 (1980).

5. J.S. Perkins, W.A. Kuperman, F. Ingenito, L.T. Fialkowski, and J. Glattetre, "Modeling Ambient Noise in 3-Dimensional Ocean Environments," *J. Acoust. Soc. Am.* **93**, 739-752 (1993).

6. R.M. Hamson, "The Theoretical Responses of Vertical and Horizontal Line Arrays to Wind-induced Noise in Shallow Water," *J. Acoust. Soc. Am.* **78**, 1702-1712 (1985).

7. T.C. Yang and K. Yoo, "Modeling the Environmental Influence on the Vertical Directionality of Ambient Noise in Shallow Water," *J. Acoust. Soc. Am.* **101**, 2541-2554 (1997).

8. B.J. Cron and C.H. Sherman, "Spatial-correlation Functions for Various Noise Models," *J. Acoust. Soc. Am.* **38**, 855 (1965).

9. C.H. Harrison, "CANARY: A Simple Model of Ambient Noise and Coherence," *Appl. Acoust.* **51**, 289-315 (1997).

10. R. Heitmeyer, S. Wales, and L. Pflug, "Propagation Model and Environmental Effects on Ship-induced Noise in the Atlantic and the Pacific: A Comparison of Two Noise Models," submitted to *J. Acoust. Soc. Am.*, 2004.

11. W. Kuperman and F. Ingenito, "Attenuation of the Coherent Component of Sound Propagating in Shallow Water with Rough Boundaries," *J. Acoust. Soc. Am.* **61**, 1178-1187 (1977).

12. S. Kirkpatrick, C.D. Gelatt, Jr., and M.P. Vecchi, "Optimization by Simulated Annealing," *Science* **220**, 671-680 (1983).